NeuroImage 339 (2026) 122169

Contents lists available at ScienceDirect

NeuroImage

journal homepage: www.elsevier.com/locate/ynimg

Distinct neural coding of action valence and intensity in the insula and amygdala

S. Ziccarelli [a,*], F. Tambuscio [a], C. Carapelli [a], G. Di Cesare [a,b]

[a] Department of Food and Drug, University of Parma, Parma, Italy
[b] Italian Institute of Technology, Cognitive Architecture for Collaborative Technologies Unit, Genova, Italy

ARTICLE INFO

Keywords:
Affective states
Vitality forms
Insula
Amygdala
Action observation
Social cognition
fMRI

ABSTRACT

In social interactions, an essential part of communication involves shaping our actions or tone of voice to convey our mood, attitude, and affect. Depending on a positive or negative attitude, an individual may perform the same action with different Vitality Forms (VFs), for instance, gently or rudely. Although VFs characterize every human action, how the brain encodes these nuances remains unclear. To address this issue, we investigated cortical and subcortical brain activity during the observation of different VFs. In particular, an fMRI study in which participants observed arm actions combined with facial expressions performed with four different VFs, varying in valence (positive or negative) and intensity (low or high), was performed. Results revealed three main findings: a) the encoding of VFs involves the activation of the dorso-central insula (DCI), middle cingulate cortex (MCC), and amygdala; b) VFs valence is encoded in the left DCI, while the VFs intensity is encoded in the amygdalae, bilaterally; c) BOLD activity was significantly associated with participants' ratings of the stimuli. Specifically, valence scores were negatively linked to activation in the insula, whereas intensity scores were positively associated with amygdala BOLD responses, suggesting a specific relationship between stimulus properties and brain activity. Together, these findings provide new insight into how the brain processes VFs conveyed simultaneously through facial and arm movements, highlighting distinct regions involved in encoding their valence and intensity and their relationship with the subjective evaluation of affective meaning.

1. Introduction

Human interactions are continuously influenced by a reciprocal interplay among affective states, moods, and attitudes. These affective processes are both shaped by and shape, in turn, how individuals perceive and engage with their surroundings. The resulting reciprocal interactions are reflected in everyday contexts, where actions carry information about the individual's internal state. Accordingly, movement becomes a crucial component of interpersonal communication, as it is modulated by the affective content that is reflected in one's actions during social interactions. One can refer to this mechanism of action modulation based on the overall internal state with the term "Vitality Forms" (VFs; Stern, 1985, 2010). This mechanism of affective modulation of our actions goes beyond the goal (*"what"*) and intention (*"why"*) of an action itself, representing instead *"how"* it is performed, an appraisal which depends on the kinematic features of the observed movement. In social interactions, this enables agents to shape their actions according to their internal states, allowing observers to infer those states from VFs features such as movement kinematics or tone of voice. Indeed, when meeting a friend, even a simple gesture such as a wave can be performed in different ways, allowing one to infer whether the greeting is genuinely affectionate or merely polite. Bodily signals, arousal, valence, motivation, as well as psychophysiological elements are some of the main components of the internal states that are the underlying mechanisms driving these dynamics. These multidimensional overall internal states enable us to integrate information about our internal physiological conditions and external environment in order to shape appropriate behavioral responses (Anderson, 2016; Bolles, 1967; Tinbergen, 1951). Therefore, VFs refer to the mechanism of expression of these states through an action, that is, the manner in which such states are expressed through and modulate motor behavior. Several neuroimaging studies aimed at investigating the neural correlates of how behavior is modulated by internal states focused on VFs. An fMRI study conducted by Di Cesare and colleagues (2014) showed that during

* Corresponding author.
E-mail addresses: settimio.ziccarelli@unipr.it (S. Ziccarelli), francesca.tambuscio@unipr.it (F. Tambuscio), cecilia.carapelli@unipr.it (C. Carapelli), giuseppe.dicesare@unipr.it (G. Di Cesare).

https://doi.org/10.1016/j.neuroimage.2026.122169
Received 30 April 2026; Received in revised form 11 July 2026; Accepted 11 August 2026
Available online 12 August 2026
1053-8119/© 2026 The Authors. Published by Elsevier Inc. This is an open access article under the CC BY license (http://creativecommons.org/licenses/by/4.0/).

the observation of actions, the action goal processing mainly activates parieto-frontal regions, whereas VFs processing leads to activation of the dorso-central sector of the insular cortex (DCI). Subsequent literature on this topic revealed that the activity of the DCI is modulated by VFs which can be conveyed not only during action observation but also during motor imagery and execution (Di Cesare et al., 2015). Furthermore, recent studies highlighted that the middle cingulate cortex (MCC), which is anatomically connected with the DCI (Di Cesare et al., 2021a) and the right amygdala (Lombardi et al., 2023), which together form a network, are involved in coding VFs aspects. While these paradigms have successfully identified the core regions involved in encoding VFs, they do not fully capture the multidimensional nature of human affective expression. In particular, these studies have focused on only two levels of action modulation, namely gentle and rude VFs expressed exclusively through arm gestures, thereby avoiding the inclusion of any other affective information that could have been conveyed by other contextual cues such as facial expressions. Against this background, the current research aims to expand the investigation on VFs modulation by introducing multiple levels and more ecological and complex visual stimuli.

Affective states are usually conceptualized through continuous, interdependent dimensions which are valence, representing a pleasure-displeasure continuum, and intensity (or arousal), representing the level of bodily activation, respectively (Posner et al., 2005). Several fMRI studies have identified that valence and intensity are coded within the insular cortex, ventromedial prefrontal cortex, anterior cingulate cortex and subcortical structures like the amygdala, in both visual and auditory modalities (Bestelmeyer et al., 2017; Fouragnan et al., 2018; Mansueto et al., 2025; Posner et al., 2009). It is worth noting that most of these investigations used static images, words, or auditory stimuli while the study of the coding of action dynamics remains underexplored although extremely relevant in everyday social interactions. In particular, it is not yet fully investigated how the DCI and amygdala, which are known to process VFs, differentially encode the valence and the intensity when upper-limb kinematics and facial expressions are integrated into a single affective display. Moreover, in naturalistic social interactions, body movements are intrinsically coupled with facial expressions, which serve as cues providing contextual information. The integration of facial expressions with bodily movements could enhance emotional perception, recruiting a distributed network of visual, prefrontal, and motor cortices, as well as the amygdala (Poyo Solanas et al., 2018). Therefore, the current research introduces a more ecological context and social approach to study the affective processing of actions. Specifically, participants were presented with videos of two agents (male and female) conveying different VFs, varying along the dimensions of valence (positive/negative) and intensity (high/low), in which arm actions (object passing) were coupled with the corresponding facial expressions. This approach will allow to investigate two fundamental key points: a) the functioning of the VFs network during the observation of more ecological stimuli characterized by both arm movement and corresponding facial expression; b) the contribution of this network to the encoding of specific VFs properties, namely their valence and intensity.

2. Materials and methods

2.1. Participants

Twenty healthy right-handed volunteers (11 females; mean age = 24.2 years, age range = 20 to 31) with no history of cognitive or neurological disorders and not receiving any psychoactive medications, took part in the fMRI experiment. Consistent with previous literature demonstrating that the effect of VFs on insula activation is robust with an average of 18 subjects using FWE cluster correction ($p < 0.05$), a sample size of 20 was deemed appropriate for this investigation (Di Cesare et al., 2025; Di Cesare et al., 2024; Lombardi et al., 2023; Di Cesare et al., 2022; Di Cesare et al., 2021a; Di Cesare et al., 2018; Di Cesare et al., 2016). All participants had normal or corrected-to-normal vision and normal hearing. Informed consent was obtained in accordance with the Helsinki declaration. The experiment was approved by the ethics committee of the University of Parma (Comitato Etico Area Vasta Emilia Nord – AVEN; code NEUROIMAGE_UNIPR).

2.2. Stimuli

Video stimuli were recorded with a video camera (Panasonic HCX 900) from a frontal perspective (180° angle, medium close-up) with a male actor and a female actress who were seated comfortably in front of a table. They were instructed to perform a passing action with their right hand toward someone sitting in front of them not visible in the frame. The sequence was the same across trials: a) starting position (index and thumb in a pinching position); b) reach-to-grasp a bottle placed in front of them; c) pass the bottle toward someone in front of them. Before performing the actions, both actors were required to experience a specific affective state and maintain an affective attitude congruent with that state towards another person sitting in front of them for at least 20 seconds and then perform the action (to grasp and pass the bottle) accordingly. To facilitate this, they imagined the other person as a close friend (positive scenario) with whom they were celebrating a special event (very positive scenario), or as someone they had argued with a few minutes earlier (negative scenario), imagining that the argument could potentially jeopardize their career permanently (very negative scenario). According to these four scenarios, a total of four corresponding actions differing in valence and intensity were performed: *positive-low; positive-high; negative-low; negative-high*. As a control condition, the two actors were required to perform the same action without a specific attitude and with a neutral facial expression (*control*). In particular, for each experimental condition, two different videos were used for the male actor and two for the actress, providing a broader set of stimuli. This was done in order to avoid possible adaptation effects to specific stimuli and maintain higher participant engagement. A white fixation cross was overlaid at the center of the video stimuli. A motion capture system (Optitrack system V12O Trio), consisting of three infrared cameras, was placed in front of the actors and used to record the action kinematic features by tracking the position of three passive markers (5 mm diameter spheres) placed on the right hand (wrist, thumb and index fingers respectively). The cameras recorded the experimental setup from a height of 2.30 m and tracked the x/y/z positions of each marker in real time using Motive software within a three-dimensional space. Data were recorded at a sampling frequency of 120 Hz, with an exposure time of 50 μs and a motion detection threshold of 160 μs. For each action, the kinetic energy ($Ek = 1/2$ mV2) required to perform the action with the object was estimated. To this purpose, both velocity and kinetic energy were calculated from the kinematic profile of the whole movement, spanning from movement onset until action completion, following the procedure validated in our previous studies (Di Cesare et al., 2014, 2016). The mass of the object (bottle = 0.350 kg) was measured and added to the mass of the actor's hand (0.5 kg) as also validated in our previously cited investigations (Di Cesare et al., 2014, 2016). It is important to note that this methodology allowed for a comparison of the kinetic energy of actions differing in valence and intensity while maintaining a constant mass across all conditions. These metrics were used to provide an objective physical validation of the intensity manipulation. By verifying that actions intended to convey high affective intensity were characterized by a greater physical kinetic energy compared to low-intensity actions, we ensured that experimental conditions were physically distinct and well-differentiated for subsequent neural analysis. The kinetic energy curves related to movements performed with the object for each combination of actor and VFs are shown in Fig. 1.

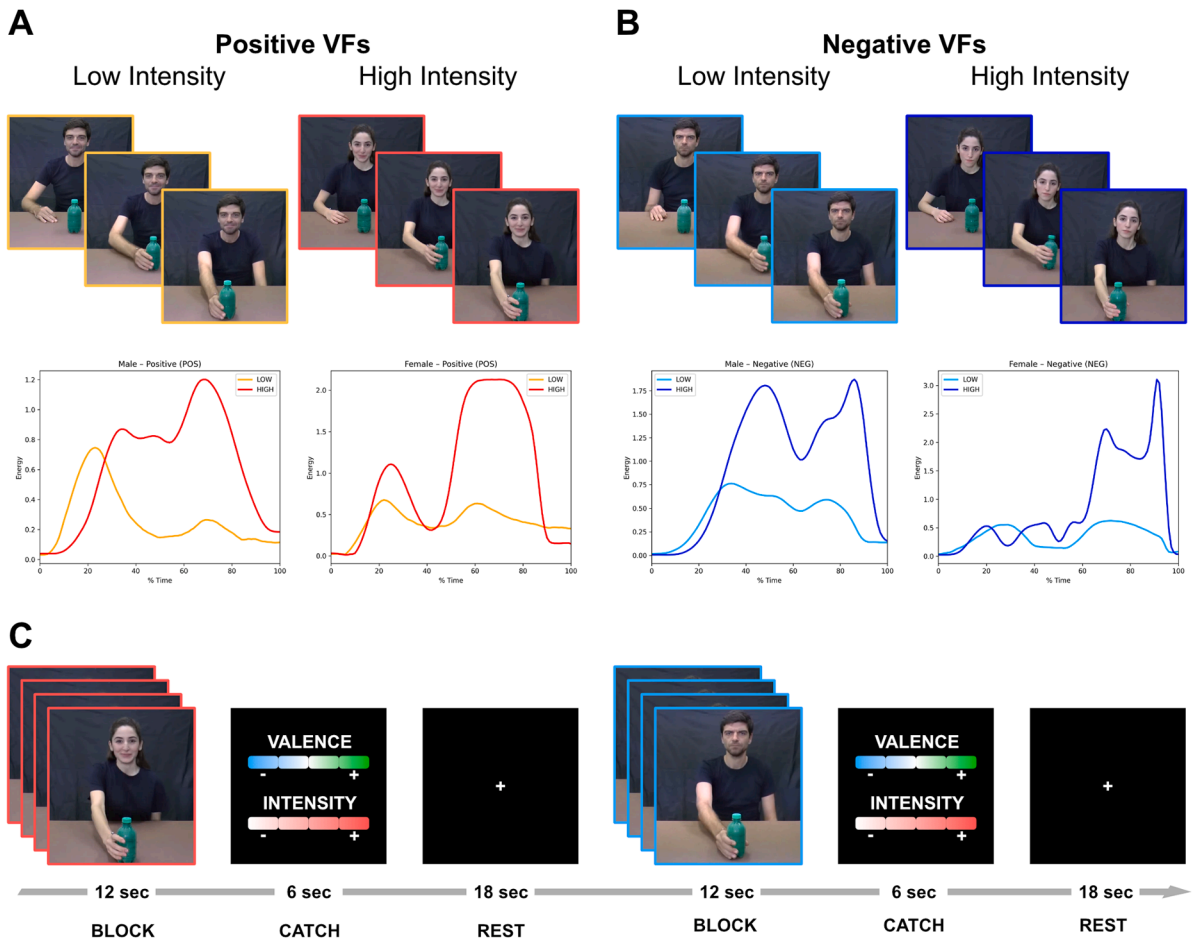


Fig. 1. Example of video frames showing the actors in the starting, grasping and final positions during the execution of the same action performed positively (A) or negatively (B). Graphs show the energy wave amplitude relative to an example of positive (warm colors) and negative action (cold colors) performed by a male actor and a female actress with low and high intensities. Experimental paradigm (C). For each condition, the experimental stimuli were presented in blocks of 4 consecutive stimuli (duration 12s) featuring videos showing actions performed by both the male actor and female actress in a randomized order to avoid potential confounding effects due to gender. This block presentation was followed by a catch trial (6s) in which participants were required to evaluate the valence (very negative, negative, positive, very positive) and the intensity (very low, low, high, very high) of the observed action. After the catch trial, a rest period (18s) was presented.

2.3. *fMRI task and design*

Before fMRI scanning, participants were briefly informed about the scanning procedure in order to help familiarize themselves with the experimental environment and setting. They were also informed that the actors in the videos would express positive or negative attitudes directly toward them using both facial expressions and bodily gestures as if interacting with them. During MR scanning, participants laid supine in the scanner in a dimly lit environment.

The experiment was performed in a single imaging acquisition session divided into 4 functional runs lasting 9 minutes each (180 volumes per run) with a total of 12 blocks for each condition presented randomly during the whole experiment. Participants were required to observe video stimuli which were presented by means of a digital goggles system (Resonance Technology, Northridge, CA) (60 Hz refresh rate) with a resolution of 800 horizontal pixels × 600 vertical pixels and horizontal eye field of 30°. Scanner noise was damped using a 30 dB noise-attenuating headset.

During the fMRI experiment, five conditions corresponding to the actions differing in *valence* and *intensity* were presented: i) *positive-low*; ii) *positive-high*; iii) *negative-low*; iv) *negative-high*; v) *control*. Each block lasted 12 s and comprised 4 videos of the same experimental or control condition. Crucially, within each block, the four videos featured actions performed by both the male actor and the female actress, presented in a randomized sequence. This specific choice was implemented to prevent any potential confounding effects or neural adaptations related to the gender of the actor. After the presentation of each block, participants were asked to rate the *valence* and *intensity* of the block of stimuli on a scale ranging from 1 = very negative to 4 = very positive for the former, and from 1 = very low to 4 = very high, for the latter. They were asked to do so by pressing a button on a response pad (NordicNeuroLab ResponseGrips) with their left thumb to decrease the value on the scale or their right thumb to increase it. Notably, this information allows to monitor participants' attention to the visual stimuli category. After each rating, an 18s signal denoising period (post-catch) was introduced to remove potential signal artifacts due to the hand movement. During this period participants had to remain still while fixating the black cross in the center of the screen (Fig. 1C). A white fixation cross at the center of the screen was overlaid during both video stimuli presentation and rest. The software E-Prime 3 Professional was used both for stimuli presentation and the recording of participants' answers.

2.4. *fMRI data acquisition*

High-resolution anatomical T1-weighted and functional T2*-weighted MR images were collected using a 3T General Electric scanner fitted with a 48-channel head coil. Functional data were acquired with a T2*-weighted gradient-echo echo-planar imaging (EPI) pulse sequence acceleration factor asset 2, 50 sequential transverse slices (slice thickness = 2.5 mm) covering the whole brain. Imaging parameters

were: TR = 3000 ms, TE = 35 ms, flip angle = 90°, and FOV = 205 × 205 mm^2. The experiment included 4 functional runs, each comprising 180 ascending interleaved volumes. In addition, a high-resolution T1-weighted structural image was obtained for each participant (acceleration factor arc 2, 200 sagittal slices, matrix 288 × 288, isotropic resolution 0.8 × 0.8 × 0.8 mm3, TR = 6900ms, TE = 2.6ms, flip angle 8°).

2.5. fMRI data preprocessing and analysis

Data analysis was performed with SPM12 (Wellcome Trust Centre for Neuroimaging, London, UK). For each participant, the functional volumes were first slice timing corrected, realigned to the mean volume and unwarped for between-scan motion correction. Subsequently, the T1-weighted image was resampled into the functional image space before segmentation into gray, white and cerebrospinal fluid, and normalization to the Montreal Neurological Institute (MNI) space, according to SPM12 pre-processing pipeline. Finally, the spatial transformations derived from the segmentation step were then applied to the realigned EPIs for normalization to the MNI space with a voxel size of 2 × 2 × 2 mm. At the end of pre-processing, all the functional normalized volumes were spatially smoothed with an 8-mm full-width half-maximum isotropic Gaussian kernel. For all participants, head motion was carefully checked along the x (pitch movement), y (yaw movement) and z (roll movement) directions; none of the participants met the exclusion criteria of 3 mm mean displacement. Data were analyzed using a random-effects model (Friston et al., 1999), implemented in a two-level procedure. In the first level, single-subject fMRI BOLD signal was modeled in two General Linear Models (GLMs) by a design-matrix comprising the onsets, the durations of each event according to the experimental task for each functional run. The GLM model was composed of six regressors corresponding to each experimental and control condition (*positive-low; positive-high; negative-low; negative-high; control*) and *catch-trial*. Notably, the BOLD signal was analyzed by using two different functions, one concerning the hemodynamic response function (HRF) and one regarding the finite impulse response (FIR). Importantly, all experimental conditions were included simultaneously within a single first-level GLM for each participant. This approach ensured that baseline variance was accounted for globally, making the FIR estimates for each condition directly comparable and preventing confounding effects deriving from separate modeling. Stimuli were presented in blocks and, within each block, videos were modelled as a whole event lasting 12s. The *catch-trial* were modeled as events lasting 12s (response 6s; post-response 6s). This was followed by a 12s rest period. In the second level analysis (group-analysis), the BOLD signal was modeled by using a GLM comprising 5 regressors (*positive-low; positive-high; negative-low; negative-high; control*). This model enabled to assess activations associated with each condition *vs.* implicit baseline (Supplementary Figure 1) and activations resulting from the direct contrast between experimental conditions and control (*positive-low vs control; positive-high vs control; negative-low vs control; negative-high vs control*) (Fig. 2 A-D). Moreover, to highlight the brain areas that play a key role in coding the *intensity* and *valence* conveyed by

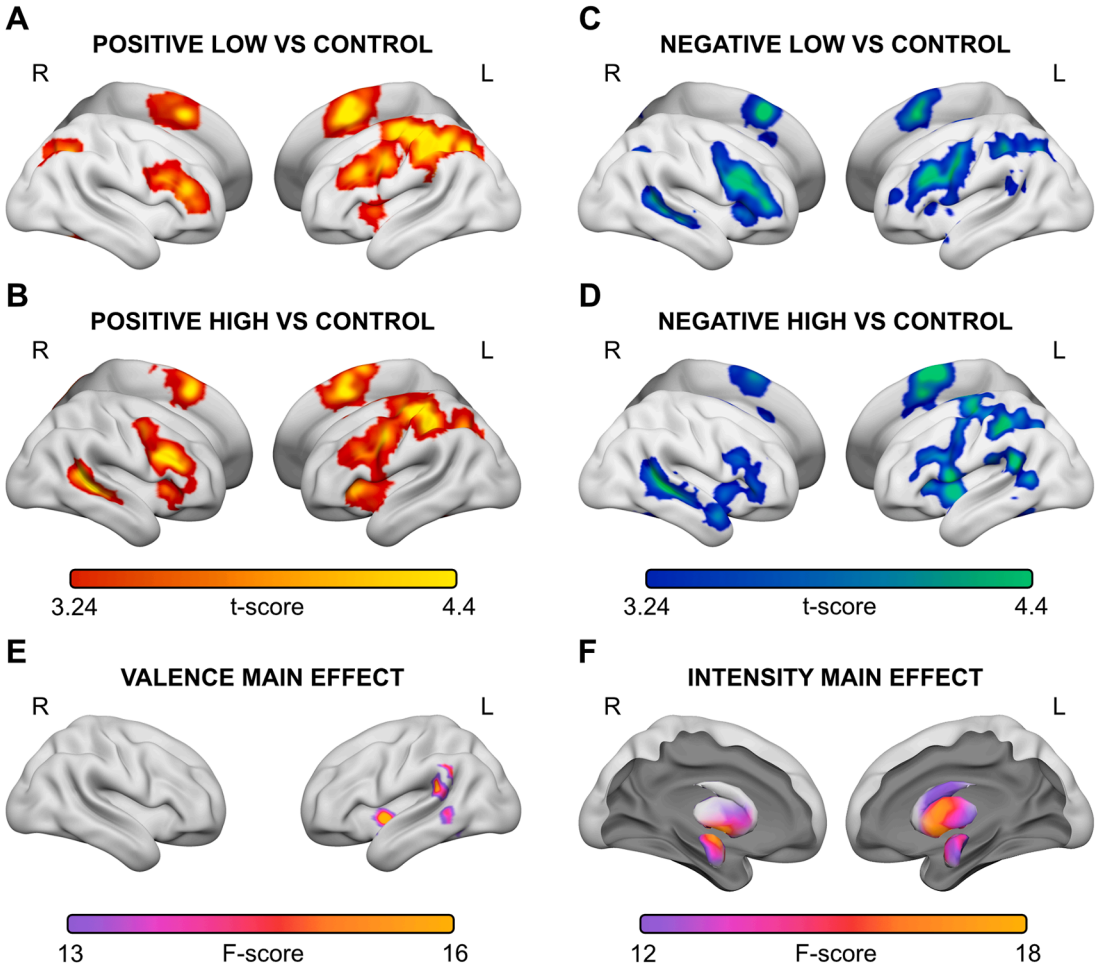


Fig. 2. Cortical activations projected onto a 3D brain template (surface; https://www.nitrc.org/projects/surfice/) identified with a significance threshold of $p < .001$ and then corrected at a cluster level using Family Wise Error (FWEc). (A) contrast between positive low vs control; (B) contrast between positive high vs control. (C) contrast between negative low vs control. (D) contrast between negative high vs control. (E) F-contrast of valence effect. (F) F-contrast of intensity effect.

the experimental stimuli, two main effect *F-contrasts* were performed (Fig. 2 E-F). Specifically, to compute the main effect of *valence* across both *intensity* levels, we applied a contrast vector of [1 1 -1 -1] assigned to the *positive-low, positive-high, negative-low,* and *negative-high* conditions, respectively. To calculate the main effect of *intensity* across both *valences*, a contrast vector of [1 -1 1 -1] was implemented for the same respective conditions. For both main effects, the statistical maps were identified at a voxel-level threshold of $p < .001$ and then corrected for multiple comparisons using Family-Wise Error at the cluster level (FWEc).

2.6. ROI analysis

To further investigate the activity of the brain areas resulting from the second level contrasts, a region of interest (ROI) analysis was carried out. ROIs were selected using an anatomical and functional approach. Specifically, as demonstrated in previous literature, the considered ROIs (DCI, MCC and amygdalae) are reliably engaged in the coding of affective processing of VFs (Di Cesare et al., 2021a, 2025; Lombardi et al., 2023). Given the theoretical focus on these areas, and that both prior studies and the results of the current research indicate their involvement in VFs coding, the investigation on the functional role of these regions is particularly relevant. For each brain region an anatomical mask was created by using the Brainnetome Atlas (https://www.nitrc.org/projects/bn_atlas; Fan et al., 2016). Specifically, the DCI (Left Insula) was defined by the Brainnetome Atlas insular subregions dIg_l, dId_l, while the MCC by the A23c_l, A24 cd_l, A6m_l, A8m_l subregions. The amygdalae were defined by the mAmyg_l, lAmyg_l subregions for the left hemisphere, and mAmyg_r, lAmyg_r for the right. Following mask creation, the BOLD signal change relative to each experimental condition (*positive-low; positive-high; negative-low; negative-high*) was extracted using SPM REX Toolbox (http://web.mit.edu/swg/rex).This analysis was carried out in order to assess possible differences between signal intensity levels within each condition (*positive-low vs positive-high; negative-low vs negative-high*) which are represented using a line plot as shown in Fig. 3. Using the same toolbox, it was possible to extract the number of activated voxels for each condition versus the control condition for each participant for each ROI. To compare paired conditions, the resulting values were subsequently tested with a Wilcoxon signed-rank test in order to assess whether there was a significant difference in cluster extension. To control for multiple comparisons across conditions and ROIs, a False Discovery Rate (FDR) correction was

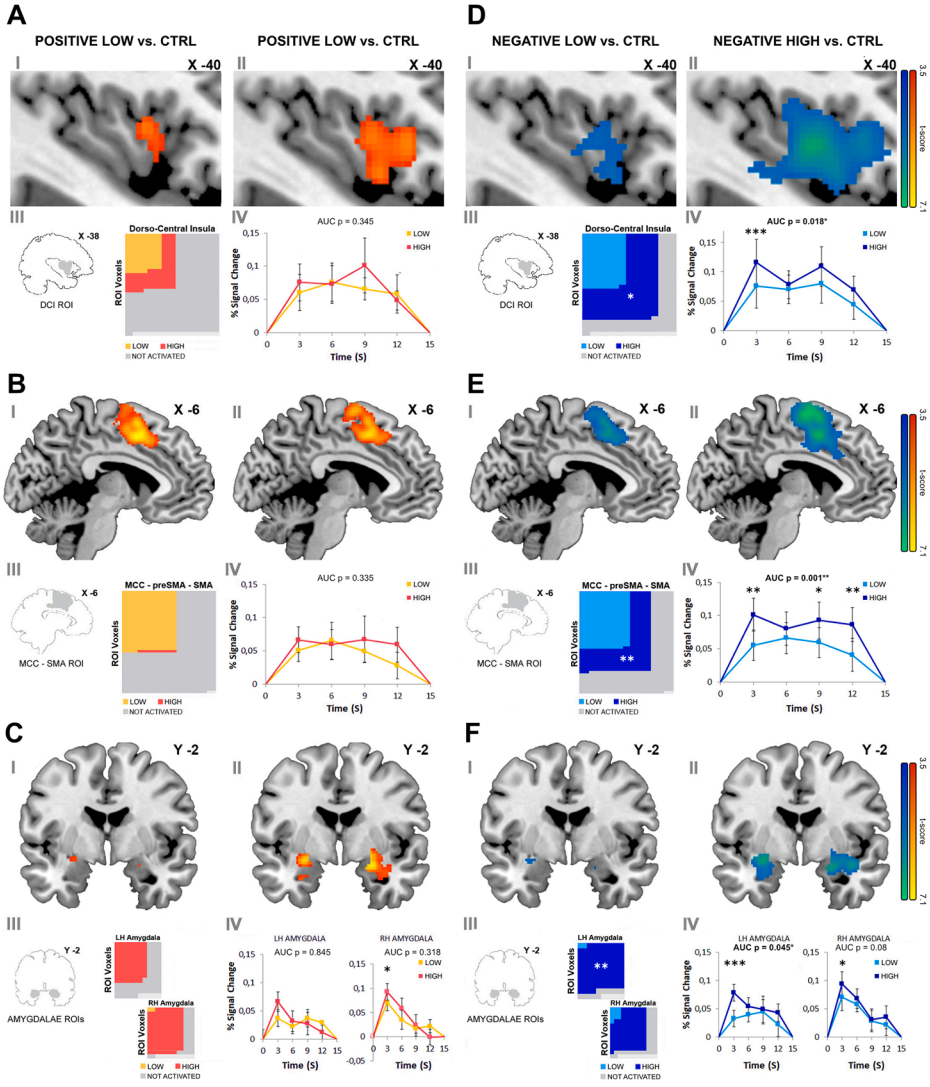


Fig. 3. Cortical and subcortical encoding of positive and negative VFs. Brain activations are rendered on MNI template sagittal and coronal slices for the contrasts of positive VFs vs. Control (A–C) and negative VFs vs. Control (D–F). Line graphs display the hemodynamic timecourses (Percent Signal Change, FIR analysis) for high (red/dark blue) and low (yellow/light blue) intensity VFs. Stacked bar charts illustrate the distribution of activated voxels within the DCI, MCC, and Amygdala, highlighting the spatial overlap between intensity levels. Asterisks indicate significant differences ($p \leq 0.05$*, ≤ 0.01**, ≤ 0.001***).

applied using the Benjamini-Hochberg procedure. Furthermore, to assess differences in BOLD signal change over time, two separate statistical approaches were implemented. First, point-by-point FDR-corrected paired t-tests were conducted across individual timepoints within each ROI. Second, the total integrated Area Under the Curve (AUC) was calculated as a single summary metric, and contrasts were evaluated using non-parametric permutation testing with 10,000 iterations.

2.7. Post-scanning behavioral task

Immediately after the fMRI scanning, participants were required to perform a behavioral task during which they observed and subsequently rated the *intensity* and *valence* of each video stimuli previously observed in the MRI scanner. Participants rated the stimuli on a continuous scale ranging from 0 to 100 where 0 = extremely low intensity/extremely negative valence and 100 = extremely high intensity/extremely positive valence. A total of 64 video stimuli were presented, 16 for each condition. This detailed investigation was fundamental to assess the perceived properties (*valence* and *intensity*) of each stimulus across participants. Furthermore, this step allowed for the study of the relation between brain activation and subjective rating of movement affect.

2.8. Affective classification

To investigate the subjective affective space and its alignment with experimental categories, a two-fold machine learning pipeline was employed using Scikit-learn library (Pedregosa et al., 2011) in Python (v3.11). Ratings of *valence* and *intensity* were first standardized using a z-score transformation to ensure comparable variance across dimensions. Firstly, using unsupervised k-means clustering, it was possible to evaluate solutions ranging from k=1 to k=7. To ensure stability against initial centroid placement, each iteration was run with 20 random initializations. The optimal cluster solution was determined using two validation metrics, namely the silhouette score (Rousseeuw, 1987) and the Davies-Bouldin index (Davies & Bouldin, 1979), calculated against 500 bootstrapped reference distributions (Chicco et al., 2025). Secondly, a Linear Discriminant Analysis (LDA) classifier was used to test the separability of the four experimental categories from the ratings. To account for the repeated-measures structure of the data and prevent data leakage, a stratified group 5-fold cross-validation scheme was performed, where data were partitioned by subject to ensure no participant's data were simultaneously present in both the training and testing sets. The significance of the decoding accuracy (chance level = 25%) was established via a permutation test with 1000 iterations.

2.9. Linear mixed models

In order to examine the relationship between neural activity and behavioral ratings, a linear mixed-effects model (LMM), which are highly robust to non-normality in the context of biological and behavioral data (Knief & Forstmeier, 2021; Schielzeth et al., 2020), was implemented using jamovi (v2.6) via the GAMLj module (Gallucci, 2019). Specifically, BOLD responses from left insula, left amygdala, and right amygdala were modeled separately as a function of standardized valence and intensity scores. Subjects were included as random intercepts to account for between-subject variability. Separate models for each region of interest were estimated via restricted maximum likelihood using the bobyqa optimizer (Powell, 2009), and degrees of freedom approximated via the Satterthwaite method (Luke, 2017). Model fit was assessed using marginal R^2 and conditional R^2_c (Nakagawa & Schielzeth, 2013). Furthermore, to test whether the predictive value of subjective affective dimensions significantly differed across the three ROIs, a subsequent LMM analysis was conducted. In this model, BOLD responses across all regions were modeled as a dependent variable, with subjects included as a random intercept. The fixed effects evaluated the direct interaction between the ROIs standardized scores of *valence* and *intensity*, using the methods described for the previous models.

3. Results

3.1. Univariate analyses

Fig. 2 shows significant activations maps overlaid on a 3D brain render, identified with a significance threshold of $p < .001$ and then corrected at a cluster level using Family Wise Error (FWEc). The cortical activation pattern deriving from the contrast *positive low vs control* shows significant clusters in the dorsolateral prefrontal cortex (dlPFC), ventral premotor cortex (PMv), part of the inferior frontal gyrus (IFG), intraparietal sulcus (IPS), middle cingulate cortex (MCC), supplementary motor (SMA) and pre-SMA areas bilaterally. Notably, in the left hemisphere, there is a significant activation pattern corresponding to the DCI, postcentral gyrus (PG) and parts of the superior parietal lobe (SPL). Cortical activation patterns, similar to those previously described, result from the contrast between *positive high* vs *control, negative low* vs *control,* and *negative high* vs *control*. Notably, DCI activation in these latter contrasts is bilateral, and the right posterior superior temporal sulcus (pSTS) is significantly activated. Furthermore, clusters of activation are present in subcortical areas such as the cerebellum, in the putamen, in the posterior part of the caudate, and in the amygdala bilaterally. F-contrasts were employed in order to investigate the main effects of *valence* and *intensity*, and activation maps were overlaid on an MNI brain template identified with a significance threshold of $p < .001$ and then corrected at a cluster level FWEc. Fig. 2E, which illustrates the main effect of valence, shows activations in left posterior STS, and superior temporal gyrus (STG), ventralmost part of the inferior parietal lobule (IPL) and left DCI. The F-contrast for intensity shows subcortical activations in the putamen, caudate, and amygdalae bilaterally (Fig. 2F). For coordinates and statistical values, see Supplementary Table 1.

Fig. 3 shows the activation patterns rendered on brain slices corresponding to the location of the ROIs coding positive (Fig. 3A-C) and negative (Fig. 3D-F) VFs compared with control conditions. The areas considered for cluster extension and BOLD signal change over time analyses are the left DCI, MCC extending to pre-SMA/SMA and left/right amygdala represented in the panels I to IV of each figure section. All reported p-values have been corrected for multiple comparisons using the Benjamini-Hochberg False Discovery Rate (FDR) procedure. In the left DCI (Fig. 3A panels I-II), the observation of both *positive low* and *positive high* VFs elicited activations in this area. While cluster size appeared more extensive for *positive high* compared to positive low conditions (Fig. 3A panel III), the analysis of cluster size did not reveal a significant difference ($t_{(19)} = 0.51$, $p = 0.520$, $d = 0.114$). Furthermore, the analysis of the BOLD signal change over time performed using FIR revealed no significant difference between these two conditions ($t_{(19)} = 0.97$, $p = 0.455$, $d = 0.218$, Fig. 3A panel IV), which was further confirmed by the AUC permutation test ($p = 0.345$). In the MCC (Fig. 3B), there was no significant difference between these conditions both for the number of activated voxels ($t_{(19)} = 1.43$, $p = 0.224$, $d = 0.320$) and for the overall BOLD activity ($t_{(19)} = 1.01$, $p = 0.455$, $d = 0.226$; Fig. 3B panel III; AUC permutation $p = 0.335$). In the left amygdala (Fig. 3C), the cluster size analysis revealed a non-significant difference both for the number of activated voxels ($t_{(19)} = 0.14$, $p = 0.332$, $d = 0.322$) and for the overall BOLD activity ($t_{(19)} = 0.224$, $p = 0.825$, $d = 0.05$; AUC permutation $p = 0.845$). Finally, in the right amygdala, cluster size analysis did not reveal a significant difference between conditions ($t_{(19)} = 2.16$, $p = 0.172$, $d = 0.484$). Similarly, overall BOLD activity did not significantly differ ($t_{(19)} = 1.03$, $p = 0.455$, $d = 0.230$; AUC permutation $p = 0.318$), although a point-by-point BOLD signal analysis revealed a localized significant difference at 3s ($t_{(19)} = 3.00$, $p = 0.029$, $d = 0.671$) (Fig. 3 panel IV).

As previously described for positive VFs, results of cluster extension and BOLD signal change over time are reported also for the observation

of negative VFs in the same regions. In the DCI, the analysis of the number of the activated voxels and of their overall BOLD activity revealed a significant difference between the *negative low* and *negative high* VFs ($t_{(19)} = 2.74$, $p = 0.017$, $d = 0.613$; $t_{(19)} = 0.59$, $p = 0.032$, $d = 0.591$, Fig. 3D). This difference was supported by the AUC permutation test ($p = 0.018$) and a point-by-point analysis showing a significant signal difference at 3s ($t_{(19)} = 5.48$, $p < 0.001$, $d = 1.226$). A similar difference in the activation pattern was also found in the MCC for cluster extension ($t_{(19)} = 3.30$, $p = 0.016$, $d = 0.737$) and overall BOLD activity ($t_{(19)} = 3.95$, $p = 0.003$, $d = 0.884$, Fig. 3E panels III and IV). The AUC permutation test further confirmed this overall difference ($p < 0.001$), and the point-by-point BOLD signal comparison indicated significant differences at 3s ($t_{(19)} = 4.63$, $p = 0.001$, $d = 1.036$), 9s ($t_{(19)} = 2.34$, $p = 0.041$, $d = 0.523$), and 12s ($t_{(19)} = 4.44$, $p = 0.001$, $d = 0.993$). In the left amygdala (Fig. 3F), the analysis revealed a significant difference for the number of activated voxels ($t_{(19)} = 3.15$, $p = 0.010$, $d = 0.704$). Although the overall BOLD activity difference became marginal after correction ($t_{(19)} = 2.08$, $p = 0.068$, $d = 0.466$), the AUC computation ($p = 0.045$) showed significant signal difference. Furthermore, the point-by-point signal analysis showed a significant difference at 3s ($t_{(19)} = 5.16$, $p < 0.001$, $d = 1.155$). Finally, no significant differences emerged in the right amygdala considering cluster extension ($t_{(19)} = 0.15$, $p = 0.881$, $d = 0.034$) and overall BOLD signal time-course ($t_{(19)} = 1.86$, $p = 0.079$, $d = 0.415$; AUC permutation $p = 0.080$), despite a localized difference at 3s ($t_{(19)} = 3.06$, $p = 0.026$, $d = 0.683$) (Fig. 3F panels III - IV).

3.2. Behavioral task analysis

The behavioral task (Fig. 4A) results revealed a clear differentiation between the four experimental categories across the valence and intensity dimensions. Descriptive analysis of the raw scores showed that valence ratings were lowest for the *negative high* (mean = 4.12; SD = 5.25) and *negative low* (mean = 22.71; SD = 9.69) conditions, while reaching maximal values in the *positive high* (mean = 87.89; SD = 7.06) and *positive low* (mean = 80.15; SD = 8.70) categories. Concerning subjective intensity scores, the *negative high* condition elicited the highest ratings (mean = 91.67; SD = 5.18), followed by *positive high* (mean = 74.99; SD = 13.32), while the *negative low* (mean = 44.50; SD = 10.68) and *positive low* (mean = 31.16; SD = 17.30) conditions were characterized by lower perceived intensity (Fig. 4B left panel).

3.3. Affective classification analysis

Unsupervised clustering provided support for a four-quadrant structure within the participants' affective ratings, consistent with the theoretical circumplex model of affect (Posner et al., 2005; Fig. 4B right panel). Analysis of the validation metrics revealed that the silhouette score reached its global maximum at k=4 (0.668), and the Davies-Bouldin index reached its global minimum (0.434), both indicating that a four-cluster solution provided the most distinct and cohesive segregation of the data. The LDA classifier successfully decoded the four stimulus categories from the dimensional ratings with a mean cross-validated accuracy of 95.0% (SD = 4.68%). Permutation testing confirmed that this performance was highly statistically significant ($p <$

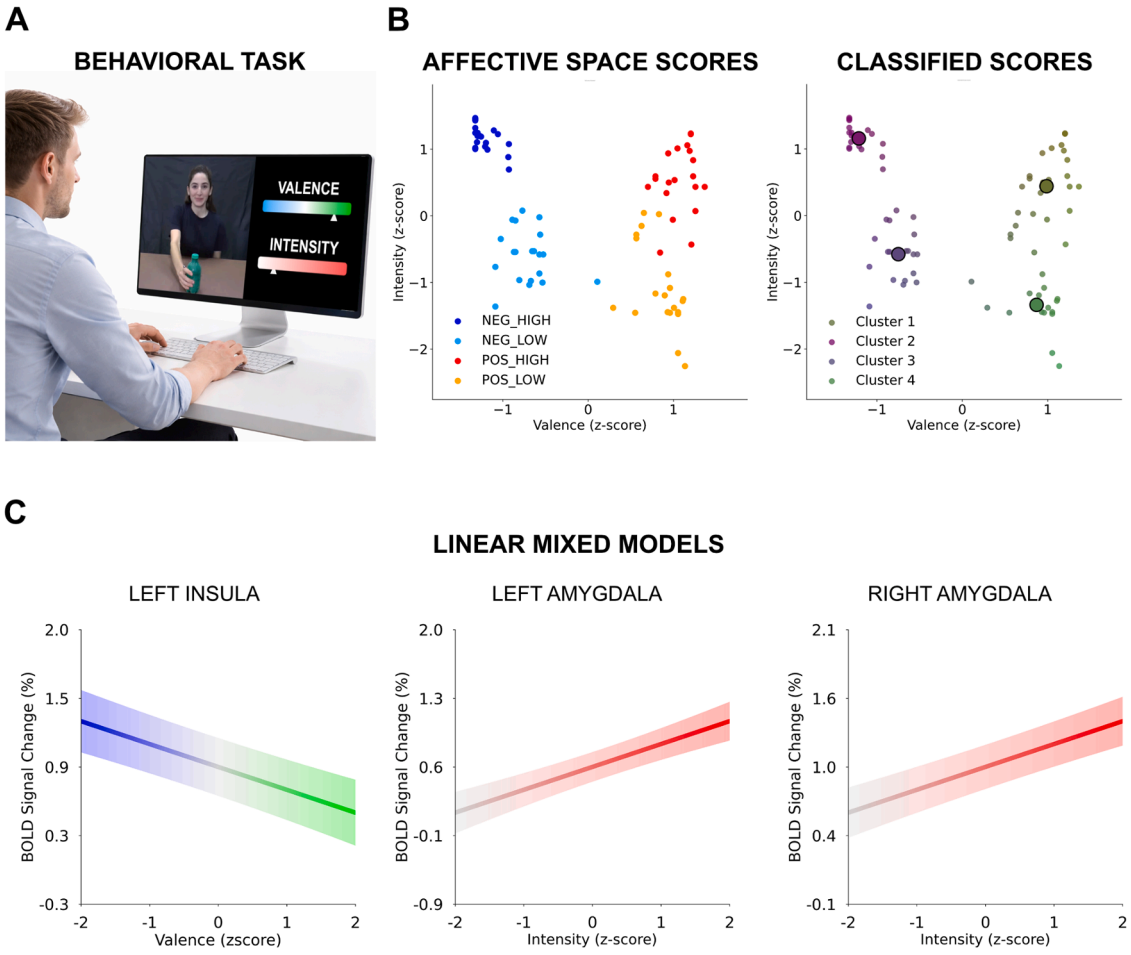


Fig. 4. (A) Experimental setup for the subjective rating task using valence and intensity visual analog scales. (B) Trial-by-trial ratings visualized in 2D affective space (left panel) and validated through unsupervised cluster analysis (right panel). (C) LMM regression plots. Shaded areas represent 95% confidence intervals.

0.001).

3.4. Linear mixed model analysis

The LMM analysis revealed a clear functional dissociation in the neural representation of subjective emotional dimensions (Fig. 4C). In the amygdala, BOLD activity was significantly associated with subjective *intensity*, with robust positive effects observed in both the right amygdala ($F_{(1,57.4)} = 17.25$, $p < 0.001$, $\beta = 0.176$) and left amygdala ($F_{(1,58.3)} = 11.63$, $p = 0.001$, $\beta = 0.229$). In these regions, *valence* did not significantly account for neural activation. Conversely, activity in the left insula was significantly predicted by subjective *valence* ($F_{(1,57.1)} = 10.70$, $p = 0.002$, $\beta = -0.229$), where lower valence scores were associated with a significant increase in BOLD signal response. Subjective *intensity ratings* did not significantly explain variance in insula activation (Table 1). In addition, a further LMM analysis performed to evaluate whether *valence* and intensity dimensions significantly differed across brain regions ($R^2 = 0.513$; $R_c^2 = 0.058$; $p < 0.001$), revealed a significant ROI × *intensity* interaction ($F_{(3,215)} = 3.79$, $p = 0.011$) and a significant ROI × *valence* interaction ($F_{(3,214)} = 3.24$, $p = 0.023$), demonstrating that the functional contributions of these affective dimensions varied significantly by region.

4. Discussion

In the present fMRI study, healthy participants observed both arm actions combined with facial expressions performed by actors conveying four different VFs, varying along the dimensions of valence (positive/negative) and intensity (low/high). Consistent with previous studies (Di Cesare et al., 2014; 2015; 2020) the current results confirm that the kinematic and affective information conveyed by the observation of pseudo-social interactions characterized by specific VFs elicits activations in a distributed network of cortical and subcortical regions. Univariate analyses reveal that observing either positive or negative VFs consistently activates the DCI, MCC and the amygdala bilaterally as well as parietal and premotor areas that are part of the Action Observation Network which not only codes kinematic features of actions (Koul et al., 2018; Ziccarelli et al., 2022, 2024) but also their affective components (Grosbras & Paus., 2006; Tamura et al., 2013; for reviews see Caspers et al., 2010; Hardwick et al., 2018; Kemmerer, 2021; Molenberghs et al., 2012). Main effect analyses showed that the DCI mainly encoded the stimuli valence whereas the amygdala encoded the stimuli intensity. Furthermore, differences in activation pattern extensions and time-course are mainly present during the observation of actions endowed with a negative affect in the abovementioned regions. Using a computational modeling approach, considering both participant's neural and behavioral responses, it was possible to further demonstrate a functional dissociation in the representations of VFs within these regions. Notably, this approach enabled us to characterize the direction of the relationship between perceived affect of observed action and the BOLD response, providing a more fine-grained account of how subjective experience maps onto neural activity. Furthermore, by combining multiple models based on *intensity* and *valence*, it was possible to assess which model better explained the relation between cortical activations and participants ratings. Specifically, BOLD activity in the left DCI was negatively associated with the perceived valence of the observed stimuli, whereas activation in both the left and right amygdalae was positively associated with their perceived intensity. These results are further supported by an LMM analysis performed to evaluate whether *valence* and *intensity* dimensions significantly differed across brain regions. These data not only corroborate the univariate results but also provide stronger evidence about the direction of the relationship between neural activity and the coding of action intensity and valence.

An important finding concerns the asymmetric processing of negative versus positive VFs. Differences in activation extent and temporal dynamics were more relevant for negative conditions. This pattern is in line with previous evidence indicating that negative stimuli elicit stronger responses due to their greater adaptive relevance (Baumeister et al., 2001; Cunningham et al., 2004). These findings are also consistent with previous VFs studies showing stronger modulation for rude or hostile actions compared to gentle ones (Di Cesare et al., 2021b). The current results extend this evidence by showing that such asymmetries persist when affect is manipulated along both valence and intensity dimensions. Therefore, modulation in neural responses is not only detectable when considering two opposite affective poles but also when considering more subtle variations. This could suggest that these areas do not merely detect valence or intensity differences within the negative or positive spectrum but actively scale their response to the degree of VFs salience or the degree of predicted unpleasantness of a social encounter with potentially adverse outcome. Interestingly, the FIR analyses, supported by the integrated AUC permutation tests and point-by-point temporal signal paired t-tests comparisons, suggest potential trends in the temporal dynamics of BOLD responses between low- and high-intensity conditions, particularly within the negative VFs. Notably, it is precisely when focusing on differences emerging in both overall temporal dynamics and point-by-point signal timecourse within the negative VFs that it is possible to hypothesize this result as an increased processing required to elaborate more salient affective features. Taken together, these results could suggest that observing actions with increasingly negative affect likely leads to a heightened processing and integration of affective and motor stimuli features , probably allowing the observer to properly respond to the agent's negative attitude.

Previous studies have shown that both insula and amygdala contribute to affective processing (Atzil et al., 2023; Lindquist et al., 2012; Malezieux et al., 2023; Pohl et al., 2013; Wang et al., 2017), yet their specific roles in encoding action-based affect remained unclear. In particular, the involvement of the amygdala in coding intensity is consistent with its established role in detecting salient and arousing stimuli (Bonnet et al., 2015; Gothard, 2014; Lin et al., 2016; Wang et al., 2017). A previous study by Lombardi and colleagues (2023) suggested an involvement of the right amygdala in encoding different VFs in participants observing video stimuli of positive facial expressions and further highlighted a link between zygomaticus major muscle activation and BOLD signal variation in the same subcortical area. The current research further deepens the knowledge about the role of this subcortical structure in coding VFs expressed in a more ecological and pseudo-social interactive setting and includes it in a potential brain

Table 1
Summary of LMM. Fixed effect estimates (β), standard errors (SE), t-statistics, and p-values are reported for the primary predictors. Marginal R-squared (R^2) represents the variance explained by the fixed effects alone, while Conditional R-squared (R_c^2) represents the variance explained by the entire model, including the random effect of Subject. Significant effects and models are highlighted in bold.

ROI	Predictor	Estimate (β)	SE	t	p	R_c^2	R^2
Left Amygdala	**Intensity**	**.229**	**.067**	**3.41**	**<.001**	.617	.067
	Valence	.032	.068	0.47	.641		
Right Amygdala	**Intensity**	**.176**	**.042**	**4.15**	**<.001**	.852	.046
	Valence	-.008	.043	-0.18	.861		
Left DCI	Intensity	.098	.069	1.42	.162	.791	.07
	Valence	**-.229**	**.07**	**-3.27**	**<.01**		

network involved in the perception of different VFs varying in intensity. Conversely, the sensitivity of the insula in encoding VFs valence, particularly to negative stimuli, supports its role in representing affective action features (for a review see Di Cesare et al., 2020), especially under conditions of negative content possibly signaling a potential threat. Its role in valence encoding and representation is supported by several works demonstrating its role in the processing of attitudes (Cunningham et al., 2004; Cerliani et al., 2025; Xiao et al., 2024). Furthermore, research by Berntson and colleagues (2011) demonstrated that lesions to the insular cortex led to a generalized reduction in the ability to assess valence across positive and negative stimuli while patients with amygdala lesions showed attenuated arousal responses primarily to unpleasant stimuli.

Taken together, the present findings not only are in line with but also enrich current literature by demonstrating that these structures differentially and parametrically encode distinct affective dimensions when information is conveyed through combined and congruent facial-upper limb movement kinematics in pseudo-social interaction contexts. Importantly, our results extend this beyond static emotional stimuli (e.g., faces or scenes) to dynamic, socially embedded VFs. The current findings further clarify VFs mechanism through which multidimensional internal states, including emotions, moods, and attitudes, are translated into action dynamics comprising facial expressions. While previous research has largely focused on neural responses to categorical emotions or static affective cues, the present results highlight that core affective brain structures are also sensitive to more nuanced VFs. This could suggest that these brain structures encode not only what someone feels, but also how that multidimensional internal state is transformed and communicated through combined facial and arm movements, contributing to a more socially relevant model of affective processing.

When observing a social interaction, affective information can derive from different effectors, such as facial expressions, upper-limb actions, or their combination. A key result of our findings lies in the multi-effector nature of our stimuli, which intentionally preserved the ecological integration of both upper-limb movements and facial expressions to convey VFs. Crucially, previous studies have shown that stimuli representing only arm actions expressing VFs consistently produce activations of the DCI, which directly corresponds to the sensorimotor functional domain (Di Cesare et al., 2015; Di Cesare et al., 2021a; Kurth et al., 2010), and MCC (Di Cesare et al., 2021a). Conversely, stimuli representing exclusively positive facial expressions, such as laughter, selectively recruit the amygdalae and the anterior short gyrus of the insula mapping onto the socio-emotional functional insular domain (Kurth et al., 2010; Lombardi et al., 2023). Extending these findings, the present study combined VFs expressed through both facial and upper-limb actions, revealing a broader network involving the DCI, MCC, amygdala, and basal ganglia. Within this network, activation of the DCI and MCC is likely related to the motor representation of the affective features of arm actions, consistent with research proposing that these regions encode the affective qualities of action kinematics and play a role in the integration of affective and motor cues (Di Cesare et al., 2021a; Portugal et al., 2020). Additionally, amygdala and anterior insular activity may be more closely associated with the processing of facial expressive cues contributing to the coding of affective intensity and valence respectively, in line with evidence suggesting that amygdalae responses to faces are modulated by salience and arousal (Lin et al., 2016, 2020; Wang et al., 2017; Bonnet et al., 2015). Therefore, our findings more precisely advance our understanding of how multimodal affective displays are processed in a pseudo-social context suggesting a dual processing stream where the DCI and MCC primarily encode valence aspects of the kinematic components of VFs, while the amygdalae's coding of intensity is likely driven by the concurrent facial expressions.

Lastly, the integration of behavioral ratings with neural data through a computational modeling approach allowed for a more direct testing of how subjective evaluations of valence and intensity relate to BOLD responses. Specifically, this approach reveals a clearer mapping between perceived affect and neural activation, providing a more fine-grained characterization of affective processing. Furthermore, this analysis allows to better clarify which neural structures are mainly involved in encoding dimensions of the stimulus features, rather than simply detecting overall differences between categories. In addition, it offers a more precise account of how combined facial expression and arm movements are encoded at the neural level in a more integrated way, consistent with recent dimensional approaches to affect representation (Cowen & Keltner, 2017; Lettieri et al., 2019).

5. Limitations and future directions

While the present study provides novel insights into the neural coding of VFs, several limitations should be considered.

First, although the stimuli were designed to enhance ecological validity by combining facial and upper-limb cues, their simultaneous presence does not allow for a clear dissociation of the respective contributions of each effector. As a result, it remains difficult to determine the extent to which facial versus arm kinematic information independently drives the observed neural responses, particularly regarding the observed parametric effects in the amygdala. Therefore, whether the amygdala parametrically encodes the intensity of a multimodal affective display or of a single effector, remains unclear. Future studies could address this limitation by isolating or manipulating the action effector conveying VFs.

Secondly, although the present study allowed for the discrimination of multiple VFs varying in valence and intensity, future research could benefit from considering a continuum of affective expressions. In particular, rather than treating positive and negative affects as discrete categories, it would be important to investigate more gradual transitions within each dimension. Indeed, social interactions rely on a continuous modulation of actions that convey affective information in a non-discrete and often subtly differentiated manner. For instance, a negative action can be expressed in multiple ways depending on internal states (e.g., mood, attitude) or contextual factors, ranging from an abrupt and explosive burst of movement to a more controlled yet rigid motor expression. Future studies could therefore explore how such continuous variations in kinematic patterns map onto neural representations at a voxel level using a multivoxel pattern analysis method (Mahmoudi et al., 2012).

Another limitation concerns the sample composition. Although the sample size ($N = 20$, 11 females) was adequate to detect the main effects of interest, it did not allow for a reliable comparison between male and female participants. While our design controlled for the gender of the actors by randomizing male and female stimuli within each presentation block, it was not possible to assess whether the observer's gender influenced the neural response to the different VFs. Future studies with larger cohorts should specifically address this question.

A final limitation concerns the characterization of dynamic interactions within the identified network. Although the present design allowed for the identification of the core nodes involved in coding VFs, it was not optimized to directly assess the causal role or the directional influences among these areas. Future studies specifically tailored for connectivity analyses, such as dynamic causal modeling (Friston et al., 2003), could more precisely characterize the functional causality within this network.

6. Conclusions

This study provides evidence on how the human brain codes action VFs when they vary in intensity and valence during pseudo-social interactions. By integrating fMRI data with behavioral ratings through computational modeling, it was possible to demonstrate a functional dissociation: a) the DCI selectively encodes the valence of an action (with heightened sensitivity to negative cues), whereas b) the bilateral

amygdalae encode the intensity of the observed multimodal affective display, showing a significant positive association with participants' intensity ratings, likely driven by concurrent facial affect rather than pure action kinematics. Furthermore, the asymmetric neural responses to negative VFs highlight an adaptive mechanism designed to process salient features of potentially adverse social encounters. Ultimately, these findings advance the understanding of social cognition by demonstrating that core affective brain structures do not merely process static emotional categories, but actively code how dynamic, multidimensional internal states are modulated and communicated through integrated bodily and facial movement.

Ethics approval statement

The study was approved by the local ethics committee (Comitato Etico Area Vasta Emilia Nord - AVEN; code NEUROIMAGE_UNIPR). This study was carried out in accordance with The Code of Ethics of the World Medical Association (Declaration of Helsinki).

CRediT authorship contribution statement

S. Ziccarelli: Conceptualization, Data curation, Formal analysis, Investigation, Methodology, Writing – original draft, Writing – review & editing. **F. Tambuscio:** Investigation, Writing – review & editing. **C. Carapelli:** Methodology, Writing – review & editing. **G. Di Cesare:** Conceptualization, Data curation, Formal analysis, Funding acquisition, Project administration, Resources, Supervision, Writing – original draft, Writing – review & editing.

Declaration of competing interest

The authors declare no competing financial or non-financial interests.

Acknowledgements

This research was funded by Ministero dell'Istruzione, dell'Università e della Ricerca under the FIS 2 Call (G.A. No. 2023-01129 to GDC). This work has been carried out in the frame of the ALIFAR project, funded by the Italian Ministry of University through the programme 'Dipartimenti di Eccellenza 2023-2027".

Supplementary materials

Supplementary material associated with this article can be found, in the online version, at doi:10.1016/j.neuroimage.2026.122169.

Data availability statement

The data of the present study can be made available, on request, from the corresponding author.

References

Anderson, D.J., 2016. Circuit modules linking internal states and social behaviour in flies and mice. Nat. Rev. Neurosci. 17, 692–704. https://doi.org/10.1038/nrn.2016.125.

Atzil, S., Satpute, A.B., Zhang, J., Parrish, M.H., Shablack, H., MacCormack, J.K., Leshin, J., Goel, S., Brooks, J.A., Kang, J., Xu, Y., Cohen, M., Lindquist, K.A., 2023. The impact of sociality and affective valence on brain activation: a meta-analysis. NeuroImage 268, 119879. https://doi.org/10.1016/j.neuroimage.2023.119879.

Baumeister, R.F., Bratslavsky, E., Finkenauer, C., Vohs, K.D., 2001. Bad is stronger than good. Rev. Gen. Psychol. 5 (4), 323–370. https://doi.org/10.1037/1089-2680.5.4.323.

Berntson, G.G., Norman, G.J., Bechara, A., Bruss, J., Tranel, D., Cacioppo, J.T., 2011. The insula and evaluative processes. Psychol. Sci. 22 (1), 80–86. https://doi.org/10.1177/0956797610391097.

Bestelmeyer, P.E., Kotz, S.A., Belin, P., 2017. Effects of emotional valence and arousal on the voice perception network. Soc. Cogn. Affect. Neurosci. 12 (8), 1351–1358. https://doi.org/10.1093/scan/nsx059.

Bolles, R.C., 1967. Theory of Motivation. Harper & Row.

Bonnet, L., Comte, A., Tatu, L., Millot, J.L., Moulin, T., Medeiros de Bustos, E., 2015. The role of the amygdala in the perception of positive emotions: an "intensity detector.". Front. Behav. Neurosci. 9, 178. https://doi.org/10.3389/fnbeh.2015.00178.

Caspers, S., Zilles, K., Laird, A.R., Eickhoff, S.B., 2010. ALE meta-analysis of action observation and imitation in the human brain. NeuroImage 50 (3), 1148–1167. https://doi.org/10.1016/j.neuroimage.2009.12.112.

Cerliani, L., Bruls, R., Teurlings, C., Ziccarelli, S., Gazzola, V., Keysers, C., 2025. Representational geometry of emotional empathy in the ventromedial prefrontal cortex and in the mid-posterior insula. BioRxiv. https://doi.org/10.1101/2025.08.30.673208.

Chicco, D., Campagner, A., Spagnolo, A., Ciucci, D., Jurman, G., 2025. The Silhouette coefficient and the Davies-Bouldin index are more informative than Dunn index, Calinski-Harabasz index, Shannon entropy, and Gap statistic for unsupervised clustering. PeerJ Comput. Sci. 11, e2221. https://doi.org/10.7717/peerj-cs.2221.

Cowen, A.S., Keltner, D., 2017. Self-report captures 27 distinct categories of emotion bridged by continuous gradients. Proc. Natl. Acad. Sci. 114 (38), E7900–E7909. https://doi.org/10.1073/pnas.1702247114.

Cunningham, W.A., Raye, C.L., Johnson, M.K., 2004. Implicit and explicit evaluation: fMRI correlates of valence, emotional intensity, and control in the processing of attitudes. J. Cogn. Neurosci. 16 (10), 1717–1729. https://doi.org/10.1162/0898929042947919.

Davies, D.L., Bouldin, D.W., 1979. A cluster separation measure. IEEE Trans. Pattern Anal. Mach. Intell. PAMI-1 (2), 224–227. https://doi.org/10.1109/TPAMI.1979.4766909.

Di Cesare, G., Di Dio, C., Rochat, M.J., Sinigaglia, C., Bruschweiler-Stern, N., Stern, D.N., Rizzolatti, G., 2014. The neural correlates of 'vitality form' recognition: an fMRI study. Soc. Cogn. Affect. Neurosci. 9 (7), 951–960. https://doi.org/10.1093/scan/nst068.

Di Cesare, G., Di Dio, C., Marchi, M., Rizzolatti, G., 2015. Expressing our internal states and understanding those of others. Proc. Natl. Acad. Sci. 112 (33), 10331–10335. https://doi.org/10.1073/pnas.1512133112.

Di Cesare, G., Valente, G., Di Dio, C., Ruffaldi, E., Bergamasco, M., Goebel, R., Rizzolatti, G., 2016. Vitality forms processing in the insula during action observation: a multivoxel pattern analysis. Front. Hum. Neurosci. 10, 267. https://doi.org/10.3389/fnhum.2016.00267.

Di Cesare, G., Gerbella, M., Rizzolatti, G., 2020. The neural bases of vitality forms. Natl. Sci. Rev. 7 (1), 202–213. https://doi.org/10.1093/nsr/nwz187.

Di Cesare, G., Marchi, M., Errante, A., Fasano, F., Rizzolatti, G., 2018. Mirroring the social aspects of speech and actions: the role of the insula. Cereb. Cortex 28 (4), 1348–1357. https://doi.org/10.1093/cercor/bhx051.

Di Cesare, G., Marchi, M., Lombardi, G., Gerbella, M., Sciutti, A., Rizzolatti, G., 2021a. The middle cingulate cortex and dorso-central insula: a mirror circuit encoding observation and execution of vitality forms. Proc. Natl. Acad. Sci. 118 (44), e2111358118. https://doi.org/10.1073/pnas.2111358118.

Di Cesare, G., Pelosi, A., Aresta, S.M., Lombardi, G., Sciutti, A., 2021b. Affective contagion: how attitudes expressed by others influence our perception of actions. Front. Hum. Neurosci. 15, 712550. https://doi.org/10.3389/fnhum.2021.712550.

Di Cesare, G., Cuccio, V., Marchi, M., Sciutti, A., Rizzolatti, G., 2022. Communicative and affective components in processing auditory vitality forms: an fMRI study. Cereb. Cortex 32 (5), 909–918. https://doi.org/10.1093/cercor/bhab254.

Di Cesare, G., Lombardi, G., Zeidman, P., Urgen, B.A., Sciutti, A., Friston, K.J., Rizzolatti, G., 2024. Two distinct networks for encoding goals and forms of action: an effective connectivity study. Proc. Natl. Acad. Sci. 121 (26), e2402282121. https://doi.org/10.1073/pnas.2402282121.

Di Cesare, G., Koush, Y., Zeidman, P., Sciutti, A., Friston, K., Rizzolatti, G., 2025. Bridging feeling and motion: insula-premotor dynamics in the processing of action vitality forms. Proc. Natl. Acad. Sci. 122 (37), e2514139122. https://doi.org/10.1073/pnas.2514139122.

Fan, L., Li, H., Zhuo, J., Zhang, Y., Wang, J., Chen, L., Yang, Z., Chu, C., Xie, S., Laird, A. R., Fox, P.T., Eickhoff, S.B., Yu, C., Jiang, T., 2016. The human Brainnetome atlas: a new brain atlas based on connectional architecture. Cereb. Cortex 26 (8), 3508–3526. https://doi.org/10.1093/cercor/bhw157.

Fouragnan, E., Retzler, C., Philiastides, M.G., 2018. Separate neural representations of prediction error valence and surprise: evidence from an fMRI meta-analysis. Hum. Brain Mapp. 39 (7), 2887–2906. https://doi.org/10.1002/hbm.24047.

Friston, K.J., Harrison, L., Penny, W., 2003. Dynamic causal modelling. NeuroImage 19 (4), 1273–1302. https://doi.org/10.1016/S1053-8119(03)00202-7.

Friston, K.J., Holmes, A.P., Price, C.J., Büchel, C., Worsley, K.J., 1999. Multisubject fMRI studies and conjunction analyses. NeuroImage 10 (4), 385–396. https://doi.org/10.1006/nimg.1999.0484.

Gallucci, M., 2019. GAMLj: General Analyses for Linear Models. jamovi module (Version 2.6.5). https://gamlj.github.io/.

Gothard, K.M., 2014. The amygdalo-motor pathways and the control of facial expressions. Front. Neurosci. 8, 43. https://doi.org/10.3389/fnins.2014.00043.

Grosbras, M.H., Paus, T., 2006. Brain networks involved in viewing angry hands or faces. Cereb. Cortex 16 (8), 1087–1096. https://doi.org/10.1093/cercor/bhj050.

Hardwick, R.M., Caspers, S., Eickhoff, S.B., Swinnen, S.P., 2018. Neural correlates of action: comparing meta-analyses of imagery, observation, and execution. Neurosci. Biobehav. Rev. 94, 31–44. https://doi.org/10.1016/j.neubiorev.2018.08.003.

Kemmerer, D., 2021. What modulates the mirror neuron system during action observation? Multiple factors involving the action, the actor, the observer, the relationship between actor and observer, and the context. Prog. Neurobiol. 205, 102128. https://doi.org/10.1016/j.pneurobio.2021.102128.

Knief, U., Forstmeier, W., 2021. Violating the normality assumption may be the lesser of two evils. Behav. Res. Methods 53 (6), 2576–2590. https://doi.org/10.3758/s13428-021-01587-5.

Koul, A., Cavallo, A., Cauda, F., Costa, T., Diano, M., Pontil, M., Becchio, C., 2018. Action observation areas represent intentions from subtle kinematic features. Cereb. Cortex 28 (7), 2647–2654. https://doi.org/10.1093/cercor/bhy098.

Kurth, F., Zilles, K., Fox, P.T., Laird, A.R., Eickhoff, S.B., 2010. A link between the systems: functional differentiation and integration within the human insula revealed by meta-analysis. Brain Struct. Funct. 214 (5–6), 519–534. https://doi.org/10.1007/s00429-010-0255-z.

Lettieri, G., Handjaras, G., Ricciardi, E., Leo, A., Papale, P., Betta, M., Pietrini, P., Cecchetti, L., 2019. Emotionotopy in the human right temporo-parietal cortex. Nat. Commun. 10 (1), 5568. https://doi.org/10.1038/s41467-019-13599-z.

Lin, H., Mueller-Bardorff, M., Mothes-Lasch, M., Buff, C., Brinkmann, L., Miltner, W.H., Straube, T., 2016. Effects of intensity of facial expressions on amygdalar activation independently of valence. Front. Hum. Neurosci. 10, 646. https://doi.org/10.3389/fnhum.2016.00646.

Lin, H., Müller-Bardorff, M., Gathmann, B., Brieke, J., Mothes-Lasch, M., Bruchmann, M., Miltner, W.H.R., Straube, T., 2020. Stimulus arousal drives amygdalar responses to emotional expressions across sensory modalities. Sci. Rep. 10 (1), 1898. https://doi.org/10.1038/s41598-020-58839-1.

Lindquist, K.A., Wager, T.D., Kober, H., Bliss-Moreau, E., Barrett, L.F., 2012. The brain basis of emotion: a meta-analytic review. Behav. Brain Sci. 35 (3), 121–143. https://doi.org/10.1017/S0140525X11000446.

Lombardi, G., Gerbella, M., Marchi, M., Sciutti, A., Rizzolatti, G., Di Cesare, G., 2023. Investigating form and content of emotional and non-emotional laughing. Cereb. Cortex 33 (7), 4164–4172. https://doi.org/10.1093/cercor/bhac334.

Luke, S.G., 2017. Evaluating significance in linear mixed-effects models in R. Behav. Res. Methods 49 (4), 1494–1502. https://doi.org/10.3758/s13428-016-0809-y.

Mahmoudi, A., Takerkart, S., Regragui, F., Boussaoud, D., Brovelli, A., 2012. Multivoxel pattern analysis for fMRI data: a review. Comput. Math. Methods Med. 2012, 961257. https://doi.org/10.1155/2012/961257.

Malezieux, M., Klein, A.S., Gogolla, N., 2023. Neural circuits for emotion. Annu. Rev. Neurosci. 46 (1), 211–231. https://doi.org/10.1146/annurev-neuro-111020-103314.

Mansueto, S.P., Romeo, Z., Angrilli, A., Spironelli, C., 2025. Emotional pictures in the brain and their interaction with the task: a fine-grained fMRI coordinate-based meta-analysis study. NeuroImage 305, 120986. https://doi.org/10.1016/j.neuroimage.2024.120986.

Molenberghs, P., Cunnington, R., Mattingley, J.B., 2012. Brain regions with mirror properties: a meta-analysis of 125 human fMRI studies. Neurosci. Biobehav. Rev. 36 (1), 341–349. https://doi.org/10.1016/j.neubiorev.2011.07.004.

Nakagawa, S., Schielzeth, H., 2013. A general and simple method for obtaining R2 from generalized linear mixed-effects models. Methods Ecol. Evol. 4 (2), 133–142. https://doi.org/10.1111/j.2041-210x.2012.00261.x.

Pedregosa, F., Varoquaux, G., Gramfort, A., Michel, V., Thirion, B., Grisel, O., Blondel, M., Prettenhofer, P., Weiss, R., Dubourg, V., Vanderplas, J., Passos, A., Cournapeau, D., Brucher, M., Perrot, M., Duchesnay, E., 2011. Scikit-learn: machine learning in Python. J. Mach. Learn. Res. 12, 2825–2830.

Pohl, A., Anders, S., Schulte-Rüther, M., Mathiak, K., Kircher, T., 2013. Positive facial affect—an fMRI study on the involvement of insula and amygdala. PLoS One 8 (8), e69886. https://doi.org/10.1371/journal.pone.0069886.

Portugal, L.C.L., Alves, R.D.C.S., Junior, O.F., Sanchez, T.A., Mocaiber, I., Volchan, E., Erthal, F.S., David, I.A., Kim, J., Oliveira, L., Padmala, S., Chen, G., Pessoa, L., Pereira, M.G., 2020. Interactions between emotion and action in the brain. NeuroImage 214, 116728. https://doi.org/10.1016/j.neuroimage.2020.116728.

Posner, J., Russell, J.A., Gerber, A., Gorman, D., Colibazzi, T., Yu, S., Wang, Z., Kangarlu, A., Zhu, H., Peterson, B.S., 2009. The neurophysiological bases of emotion: an fMRI study of the affective circumplex using emotion-denoting words. Hum. Brain Mapp. 30 (3), 883–895. https://doi.org/10.1002/hbm.20553.

Posner, J., Russell, J.A., Peterson, B.S., 2005. The circumplex model of affect: an integrative approach to affective neuroscience, cognitive development, and psychopathology. Dev. Psychopathol. 17 (3), 715–734. https://doi.org/10.1017/S0954579405050340.

Powell, M.J.D., 2009. The BOBYQA Algorithm for Bound Constrained Optimization Without Derivatives. University of Cambridge (Report No. DAMTP 2009/NA06).

Poyo Solanas, M., Zhan, M., Vaessen, M., Hortensius, R., Engelen, T., de Gelder, B., 2018. Looking at the face and seeing the whole body: neural basis of combined face and body expressions. Soc. Cogn. Affect. Neurosci. 13 (1), 135–144. https://doi.org/10.1093/scan/nsx130.

Rousseeuw, P.J., 1987. Silhouettes: a graphical aid to the interpretation and validation of cluster analysis. J. Comput. Appl. Math. 20, 53–65. https://doi.org/10.1016/0377-0427(87)90125-7.

Schielzeth, H., Dingemanse, N.J., Nakagawa, S., Westneat, D.F., Allegue, H., Teplitsky, C., Réale, D., Dochtermann, N.A., Garamszegi, L.Z., Araya-Ajoy, Y.G., 2020. Robustness of linear mixed-effects models to violations of distributional assumptions. Methods Ecol. Evol. 11 (9), 1141–1152. https://doi.org/10.1111/2041-210X.13434.

Stern, D.N., 1985. The Interpersonal World of the Infant. Basic Books.

Stern, D.N., 2010. Forms of Vitality: Exploring Dynamic Experience in Psychology, Arts, Psychotherapy, and Development. Oxford University Press.

Tamura, M., Moriguchi, Y., Higuchi, S., Hida, A., Enomoto, M., Umezawa, J., Mishima, K., 2013. Activity in the action observation network enhances emotion regulation during observation of risk-taking: an fMRI study. Neurol. Res. 35 (1), 22–28. https://doi.org/10.1179/1743132812Y.0000000109.

Tinbergen, N., 1951. The Study of Instinct. Clarendon Press.

Wang, S., Yu, R., Tyszka, J.M., Zhen, S., Kovach, C., Sun, S., Huang, Y., Hurlemann, R., Ross, I.B., Chung, J.M., Mamelak, A.N., Adolphs, R., Rutishauser, U., 2017. The human amygdala parametrically encodes the intensity of specific facial emotions and their categorical ambiguity. Nat. Commun. 8, 14821. https://doi.org/10.1038/ncomms14821.

Xiao, J., Adkinson, J.A., Allawala, A.B., Banks, G., Bartoli, E., Fan, X., Mocchi, M., Pascuzzi, B., Pulapaka, S., Franch, M.C., Mathew, S.J., Mathura, R.K., Myers, J., Pirtle, V., Provenza, N.R., Shofty, B., Watrous, A.J., Pitkow, X., Goodman, W.K., Pouratian, N., Sheth, S., Bijanki, K.R., Hayden, B.Y., 2024. Insula uses overlapping codes for emotion in self and others. BioRxiv. https://doi.org/10.1101/2024.06.04.596966.

Ziccarelli, S., Errante, A., Fogassi, L., 2022. Decoding point-light displays and fully visible hand grasping actions within the action observation network. Hum. Brain Mapp. 43 (14), 4293–4309. https://doi.org/10.1002/hbm.25954.

Ziccarelli, S., Errante, A., Fogassi, L., 2024. Direction and velocity kinematic features of point-light displays grasping actions are differentially coded within the action observation network. NeuroImage 303, 120939. https://doi.org/10.1016/j.neuroimage.2024.120939.